Turbulence Models for Compressible Disperse Multiphase Flows

Rodney O. Fox[1,2(✉)]

[1] Department of Chemical and Biological Engineering, Iowa State University, Ames, IA 50011-1098, USA
rofox@iastate.edu

[2] Center for Multiphase Flow Research and Education, Iowa State University, Ames, IA 50011-1096, USA

Abstract. Multiphase turbulence driven by coupling between the phases can arise in the absence of mean shear. For example, due to gravity (or other body forces) in disperse multiphase flows (e.g., particle-laden and bubbly flows), the mean-slip velocity between phases and spontaneous cluster formation generate strong turbulence that is nearly one dimensional. Such complex flows can be modeled using Eulerian–Eulerian two-fluid models. Here, starting from a compressible two-fluid model, a Reynolds-averaged turbulence model is derived for disperse multiphase flows driven by gravity. Due to the diagonal form of the Reynolds-stress tensors, the model equations are hyperbolic and thus require time-dependent solutions and dedicated numerical solvers.

Keywords: disperse multiphase flow · turbulence modeling · hyperbolic two-fluid model

1 Introduction

Multiphase turbulence takes many different forms and arises in many different contexts [1–10]. Here, we will consider only disperse multiphase flows with a discrete phase (e.g., solid particles, droplets or bubbles) and a continuous fluid phase. Furthermore, for simplicity, we will focus on cases where the disperse-phase elements are identical, i.e., have the same material density and geometry. In other words, we will consider only monodisperse multiphase flows. Even with these restrictions, disperse multiphase turbulent flows can be further categorized into two broad classes: (i) flows where the turbulence originates in the continuous phase with the discrete phase modulating the small scales of the turbulence [11–17], and (ii) flows where the turbulence arises due to the coupling between the discrete and continuous phases. The former is often associated with particle-laden turbulent flows and its study is mainly focused on how the discrete phase modifies the classical turbulence structures seen in single-phase flows. The latter, which is the topic of this work, can be observed in gas–particle flows when the

X. Zheng and S. Balachandar (Eds.): IUTAM 2023, IUTAM Bookseries 41, pp. 117–140, 2024.
https://doi.org/10.1007/978-3-031-47258-9_7

mass of the particles is of the same order or greater than that of the gas phase; or in bubbly flows when the bubble volume fraction is high enough to lead to buoyancy-driven instabilities.

The remainder of the work is organized as follows. First, we present the Eulerian–Eulerian (EE) two-fluid model for compressible disperse multiphase flows developed in [18,19] (but not considering pseudoturbulence nor particle internal energy for the sake of clarity). Next, we describe the Reynolds-averaged turbulence model that results from the EE model after averaging and applying closures. This turbulence model is our main result, and care is taken to ensure that it is globally hyperbolic (as described in [18]). As an application, we then reduce the model equations for the case of statistically stationary, homogeneous turbulence driven by gravity (e.g., cluster-induced turbulence (CIT) [20] and buoyancy-driven turbulence (BDT) [21]). The paper concludes with some general remarks concerning multiphase turbulence models and open questions.

2 Compressible Two-Fluid Model

The starting point for formulating the turbulence model is the inviscid, compressible two-fluid model in Table 1. As discussed in detail in [18,19], this model accounts for added mass by allowing a portion of the fluid with volume fraction $\alpha_a = \alpha_p^\star - \alpha_p$ to move with the particle-phase velocity $\mathbf{u}_p$. The particle material density ρ_p is constant, while the fluid density ρ_f varies due to compression/expansion. The particle-phase volume fraction is α_p, and $\alpha_f = 1 - \alpha_p$ is that of the fluid phase.

2.1 Mass

In the mass balances, the source term S_a models fluid exchange between the particle wakes and the bulk fluid. The latter has velocity $\mathbf{u}_f$ and volume fraction $\alpha_f^\star$. As demonstrated in [18], treating the added mass is this manner is exactly equivalent to the virtual-mass force used in two-fluid modeling, but has the advantage of ensuring that the model is hyperbolic for arbitrary material-density ratios $Z = \rho_f/\rho_p$. Thus, the model in Table 1 is applicable to gas–particle flows with $\rho_p \gg \rho_f$, as well as to bubbly flows with $\rho_p \ll \rho_f$ or suspensions with $\rho_p \approx \rho_f$. In order to allow for large-density fluids (e.g., water or other liquids), the fluid equation of state (EOS) is modeled as a stiffened gas:

$$p_f = \rho_f(\gamma_f - 1)\Theta_f - \gamma_f p_f^o, \tag{1}$$

but any other EOS could be used as well. The conserved variables in the mass balances are

$$(X_1, X_2, X_3) = (\alpha_p, \rho_e \alpha_p^\star, \rho_f \alpha_f^\star) \tag{2}$$

where ρ_e is the effective density of the particle with its added mass. Thus, the volume fractions and fluid density are found from the conserved variables by

$$(\alpha_p, \rho_f, \alpha_a) = \left(X_1, \frac{X_3 + X_2 - \rho_p X_1}{\alpha_f}, \frac{X_2 - \rho_p X_1}{\rho_f} \right). \tag{3}$$

Finally, to enforce the limit $0 \leq \alpha_a \leq \alpha_f$, a new variable c_m is introduced such that $\alpha_a = c_m \alpha_f \alpha_p$. In the very dilute limit, c_m corresponds to the virtual-mass constant, whose value is 0.5 for spherical particles. The latter is imposed in the model for S_a using the parameter $c_m^\star$. In summary, the two-fluid model in Table 1 contains three mass balances in order to account for added mass while remaining globally hyperbolic [18,19].

2.2 Momentum

The two momentum balances in Table 1 use the two conserved variables

$$(X_4, X_5) = (\rho_e \alpha_p^\star \mathbf{u}_p, \rho_f \alpha_f^\star \mathbf{u}_f), \tag{4}$$

which correspond, respectively, to the momentum of the particles with the added mass, and to the momentum of the bulk fluid.[1] The phase velocities are related to the conserved variables by

$$(\mathbf{u}_p, \mathbf{u}_f) = \left(\frac{X_4}{X_2}, \frac{X_5}{X_3} \right). \tag{5}$$

In addition to the fluid pressure p_f and the particle pressure p_p, a pressure contribution due to the slip-velocity tensor R appears for the particle phase. This particle-fluid-particle ($_{pfp}$) pressure tensor P_{pfp} arises in the kinetic theory derivation of a binary system [22], and is nonzero whenever the slip velocity $\mathbf{u}_{fp}$ is nonzero. As shown in [22], it plays an important role in gas–particle flows to ensure that the system is hyperbolic. The particle pressure p_p is the sum of two contributions. The first is the usual collisional pressure that depends on particle-phase granular temperature Θ_p. The second is the frictional or elastic pressure for close-packed particles ($\alpha_p > 0.63$) that depends on α_p only. The parameter p_c is set to a large value to resist increases in α_p once the particles are in contact. The latter is controlled by the tanh function, which provides a sharp transition near $\alpha_p = 0.6$. Note that this pressure contribution is present in dense flows such as fluidized beds, but will be absent for riser flows where $\alpha_p \ll 0.63$. For frictional particles, by including a interparticle-friction dependence and a saltation model in the particle pressure and viscous terms (which are neglected here), good agreement with discrete particle simulations of dense liquid–particle flows has been reported in the literature [23].

The source terms on the right-hand sides of the momentum balances represent, respectively, fluid drag; buoyancy; forces due to fluid density gradients, expansion/contraction, and mean shear (e.g., lift); momentum transfer due to added mass; and gravity. The drag coefficient C_D depends on Re_p and α_p and a correlation [24] must be provided to complete the model, e.g., $C_D Re_p = 24$

[1] As discussed in [18], the total fluid velocity $\mathbf{v}_f$ is related to the bulk fluid velocity by $\alpha_f \mathbf{v}_f = \alpha_a \mathbf{u}_p + \alpha_f^\star \mathbf{u}_f$. Thus, depending on the value of α_a, the turbulence statistics will be different for the bulk and total fluid. In most two-fluid simulations [21], the statistics are computed using $\mathbf{v}_f$.

Table 1. Inviscid, compressible two-fluid model for monodisperse elastic particles in a fluid modeled as a stiffened gas with parameters γ_f and p_f^o [18]. The drag coefficient, C_D, depends on Re_p and α_p. The slip-velocity tensor R is the exact expression from kinetic theory and defines the pfp-pressure tensor P_{pfp}.

Mass

$$\begin{aligned}\partial_t\alpha_p + \partial_{\mathbf{x}}\cdot(\alpha_p\mathbf{u}_p) &= 0\\ \partial_t(\rho_e\alpha_p^\star) + \partial_{\mathbf{x}}\cdot(\rho_e\alpha_p^\star\mathbf{u}_p) &= S_a\\ \partial_t(\rho_f\alpha_f^\star) + \partial_{\mathbf{x}}\cdot(\rho_f\alpha_f^\star\mathbf{u}_f) &= -S_a\end{aligned}$$

Momentum

$$\begin{aligned}\partial_t(\rho_e\alpha_p^\star\mathbf{u}_p) + \partial_{\mathbf{x}}\cdot(\rho_e\alpha_p^\star\mathbf{u}_p\mathbf{u}_p + p_p\mathsf{I} + \mathsf{P}_{pfp}) &= K\mathbf{u}_{fp} - \alpha_p^\star(\partial_{\mathbf{x}}p_f + \mathbf{F}_{pf}) + \mathbf{S}_{fp} + \rho_e\alpha_p^\star\mathbf{g}\\ \partial_t(\rho_f\alpha_f^\star\mathbf{u}_f) + \partial_{\mathbf{x}}\cdot(\rho_f\alpha_f^\star\mathbf{u}_f\mathbf{u}_f + p_f\mathsf{I}) &= K\mathbf{u}_{pf} + \alpha_p^\star(\partial_{\mathbf{x}}p_f + \mathbf{F}_{pf}) - \mathbf{S}_{fp} + \rho_f\alpha_f^\star\mathbf{g}\end{aligned}$$

Total Energy

$$\begin{aligned}&\partial_t(\rho_e\alpha_p^\star E_p) + \partial_{\mathbf{x}}\cdot(\rho_e\alpha_p^\star E_p\mathbf{u}_p + p_p\mathbf{u}_p + \mathsf{P}_{pfp}\cdot\mathbf{u}_p) = \mathsf{P}_{pfp} : \partial_{\mathbf{x}}\mathbf{u}_p\\ &- K\left(3\Theta_p + \mathbf{u}_p\cdot\mathbf{u}_{pf}\right) - \alpha_p^\star\mathbf{u}_p\cdot(\partial_{\mathbf{x}}p_f + \mathbf{F}_{pf}) + S_E + \rho_e\alpha_p^\star\mathbf{u}_p\cdot\mathbf{g}\end{aligned}$$

$$\begin{aligned}&\partial_t(\rho_f\alpha_f^\star E_f) + \partial_{\mathbf{x}}\cdot[\rho_f\alpha_f^\star E_f\mathbf{u}_f + (\alpha_f^\star\mathbf{u}_f + \alpha_p^\star\mathbf{u}_p)p_f] = -\mathsf{P}_{pfp} : \partial_{\mathbf{x}}\mathbf{u}_p\\ &+ K\left(3\Theta_p + \mathbf{u}_p\cdot\mathbf{u}_{pf}\right) + \alpha_p^\star\mathbf{u}_p\cdot(\partial_{\mathbf{x}}p_f + \mathbf{F}_{pf}) - S_E + \rho_f\alpha_f^\star\mathbf{u}_f\cdot\mathbf{g}\end{aligned}$$

where

$$\alpha_f + \alpha_p = 1 \quad \alpha_f^\star + \alpha_p^\star = 1 \quad \alpha_p^\star = \alpha_p + \alpha_a \quad \rho_e = \frac{\rho_p\alpha_p + \rho_f\alpha_a}{\alpha_p + \alpha_a}$$

$$\mathbf{u}_{fp} = -\mathbf{u}_{pf} = \mathbf{u}_f - \mathbf{u}_p \quad K = \frac{3\rho_e\alpha_p^\star C_D Re_p}{4\tau_p} \quad \tau_p = \frac{\rho_e d_p^2}{\mu_f} \quad Re_p = \frac{\alpha_f^\star}{\alpha_f}\frac{d_p u_{fp}}{\nu_f}$$

$$S_a = \frac{\rho_f}{\tau_a}(c_m^\star\alpha_f\alpha_p - \alpha_a) \quad \mathbf{S}_{fp} = \max(S_a, 0)\mathbf{u}_f + \min(S_a, 0)\mathbf{u}_p$$

$$S_E = \max(S_a, 0)\frac{1}{2}u_f^2 + \min(S_a, 0)E_p \quad \tau_a = \frac{4d_p^2}{3\nu_f C_D Re_p} \quad c_m^\star = \frac{1}{2}\min(1 + 2\alpha_p, 2)$$

$$\mathbf{F}_{pf} = \mathsf{R}\cdot\partial_{\mathbf{x}}\rho_f - \rho_f(\gamma_f - 1)tr(\mathsf{\Gamma})\mathbf{u}_{fp} + \frac{4}{5}\rho_f\mathsf{S}\cdot\mathbf{u}_{fp} \quad \mathsf{R} = \frac{1}{5}u_{fp}^2\mathsf{I} + \frac{2}{5}\mathbf{u}_{fp}\mathbf{u}_{fp}$$

$$\mathsf{\Gamma} = \frac{1}{2}\left[\partial_{\mathbf{x}}\mathbf{u}_f + (\partial_{\mathbf{x}}\mathbf{u}_f)^t\right] \quad \mathsf{S} = \mathsf{\Gamma} - \frac{1}{3}tr(\mathsf{\Gamma})\mathsf{I}$$

$$p_f = \rho_f(\gamma_f - 1)\Theta_f - \gamma_f p_f^o \qquad \mathsf{P}_{pfp} = C_{pfp}\rho_f\alpha_p^\star\mathsf{R} \quad C_{pfp} = c_m^\star$$

$$p_p = \rho_e\alpha_p^\star\Theta_p(1 + 4\alpha_p g_0) + p_c\alpha_p g_0\frac{1}{2}\left[1 + \tanh\left(\frac{\alpha_p - 0.6}{0.01}\right)\right] \quad g_0 = \frac{1 + \alpha_f}{2\alpha_f^3}$$

$$\Theta_f = E_f - \frac{1}{2}u_f^2 \quad \Theta_p = \frac{2}{3}\left(E_p - \frac{1}{2}u_p^2\right)$$

for Stokes drag. As shown in [18], P_{pfp} is crucial for ensuring that the system is globally hyperbolic for bubbly flows and for gas–particles flows when, e.g., the granular temperature Θ_p is negligible. Note that P_{pfp} scales like $\alpha_p^\star$ (i.e., it is first order in particle concentration[2]) and corresponds to particle–particle interactions mediated by the fluid. For global hyperbolicity for any Z, the parameter C_{pfp} is set equal to $c_m^\star$, but smaller values can be used in gas–particle flows.

2.3 Total Energy

The total energy balances in Table 1 are written in terms of the two conserved variables

$$(X_6, X_7) = (\rho_e \alpha_p^\star E_p, \rho_f \alpha_f^\star E_f), \tag{6}$$

and thus the specific total energies are related to the conserved variables by

$$(E_p, E_f) = \left(\frac{X_6}{X_2}, \frac{X_7}{X_3}\right). \tag{7}$$

For the particle phase (including the added mass), the internal energy is not included in the total energy, implying that the phase is adiabatic. This is possible when the particle–particle collisions are assumed elastic. When inelastic collisions are required (e.g., high-speed gas–particle flows [24]), then the energy dissipation term in the particle phase would appear as a source term in the particle-phase internal energy balance [19]. The granular temperature Θ_p corresponds to the particle velocity fluctuations relative to the mean velocity $\mathbf{u}_p$. In contrast, the fluid-phase thermodynamic temperature is proportional to its internal energy Θ_f. The relationship between these temperatures and the total energies are given in Table 1 where γ_f is the heat-capacity ratio for the fluid.

As shown in [22], kinetic theory provides closed forms for the energy fluxes. The total energy flux for the particle phase has the classical form of an ideal gas, but with an additional contribution due to the pfp-pressure tensor. For the fluid phase an additional energy-flux term appears due to the presence of the particle phase. Note that $(\alpha_f^\star \mathbf{u}_f + \alpha_p^\star \mathbf{u}_p)$ is the volume-average velocity of the fluid–particle mixture, which sees the continuous phase pressure p_f. The source terms on the right-hand sides of the total energy balances represent, respectively, the work done by the fluid on the particles to lower α_p due to the pressure P_{pfp},[3] fluid drag, buoyancy, work done by forces $\mathbf{F}_{pf}$, potential energy, and mass transfer. Many of these terms represent energy exchange from the particle phase to the fluid phase (i.e., fluid heating and pseudoturbulence [18,19]). Here, we neglect pseudoturbulence and focus on large-scale multiphase turbulence accompanied by fluctuations in α_p (i.e., cluster-induced and buoyancy-driven turbulence). A two-fluid model that includes heat transfer and pseudoturbulence can be found in [19].

[2] A second-order model is also analyzed in [18].

[3] Using the mass balance for α_p, $\partial_{\mathbf{x}} \cdot \mathbf{u}_p$ can be replaced by the rate of change of α_p as it moves with velocity $\mathbf{u}_p$.

For systems with inelastic collisions and/or strong fluid drag, the granular temperature can be very small and care must be taken to ensure that numerical errors do not result in negative Θ_p when it is found by subtracting the mean kinetic energy $\frac{1}{2}u_p^2$ from E_p. Alternatively, a non-conservative equation for Θ_p:

$$\frac{3}{2}\partial_t(\rho_e\alpha_p^\star\Theta_p) + \frac{3}{2}\partial_{\mathbf{x}}\cdot(\rho_e\alpha_p^\star\Theta_p\mathbf{u}_p) = -p_p\partial_{\mathbf{x}}\cdot\mathbf{u}_p - 3K\Theta_p \tag{8}$$

could be employed. Note that this equation does not depend on P_{pfp}, and is valid for elastic collisions and $\alpha_p \ll 0.63$. For inelastic collisions or larger α_p, dissipation terms appear that change the particle-phase internal energy [19]. In practice [19], when the conservative form is used to solve for E_p, it suffices to clip Θ_p to non-negative values when evaluating terms on which it depends. This is possible because when Θ_p is negligible, the eigenvalues of system are real-valued due to P_{pfp} and, hence, the fluxes are non-degenerate. In most applications, the eigenvalues associated with p_f will be much larger than those associated with the particle phase, especially if the fluid phase is a liquid. For reference, when $Z \approx 0$ (e.g., gas–particle flows), the particle-phase speed of sound is $\sqrt{5\Theta_p/3}$ [18]. Thus, the particle-phase Mach number can correspond to hypersonic flow when Θ_p is small. This is also approximately true for larger values of Z where other physical mechanisms in addition to drag are important (e.g., buoyancy).

2.4 Summary

In summary, the two-fluid model in Table 1 is the starting point for developing a turbulence model for compressible disperse multiphase flows. Aside from the body force $\mathbf{g}$, these equations conserve mass, momentum and total energy for the mixture, i.e., by summing together the two equations representing each phase. As shown in [18,19], this model is globally hyperbolic and can be solved using numerical methods for hyperbolic conservation laws [25]. Nonetheless, the wide range of timescales appearing in the fluxes (especially for liquids) make the numerical solution challenging from the point of view of their cost. In high-speed multiphase flows, the fluid-phase Mach number will be very large, implying that shocks will be present in the solutions. As in single-phase flows, shock-resolving solutions require fine grids (at least locally near the shock). In contrast, in gravity-driven flows the fluid phase usually has a low Mach number and the fluid density ρ_f can be treated as constant, eliminating the need for the fluid-phase total energy balance [18].

The principal objective when developing a turbulence model will be to reduce the grid-resolution requirement due to 'turbulent viscosity/diffusion' and by decreasing the particle-phase Mach number. Indeed, as the eigenvalues of the fluid phase will not be significantly changed (or removed by taking ρ_f constant) in the turbulence model, a coarser grid will allow for larger time steps while still satisfying the CFL condition. Nonetheless, even after phase averaging, the system must remain hyperbolic and large temporal variations in the volume fraction will not be damped out. Thus, the model will usually not exhibit stable time-independent solutions unless the particle-phase Mach number is very small.

3 Multiphase Turbulence Model

The turbulence model in Table 2 is found by phase averaging the two-fluid model in Table 1 following the method presented in [26,27]. During this process, numerous unclosed terms are introduced that require physics-based closures. The turbulence model in Table 2 is the final closed form, and care has been taken to ensure that the closures for the fluxes do not change the hyperbolicity of the system. We remind the reader that only terms involving space and time derivatives influence the hyperbolicity. Thus, the closures for point-wise source terms do not affect the eigenvalues and, hence, more latitude is available when choosing their mathematical forms. In general, we have chosen forms that attempt to capture the behavior of cluster-induced (CIT) and buoyancy-driven (BDT) turbulence [27]; however, turbulence arising due to mean shear is also included. At this stage, we consider only the simplest forms for the Reynolds-stress transport equations corresponding to linear relaxation. Likewise, the spatial transport of scalar quantities due to turbulent fluctuations is modeled using a gradient-transport model [28]. For clarity and simplicity, we drop the subscripts introduced in [26] to denote phase averages, and give the final closed forms for the turbulence model developed in [27].

One important point that is often underestimated in multiphase turbulence models is that for CIT and BDT the phasic Reynolds stresses are nearly one-dimensional turbulence [28]. In other words, the shear stress components are very small, implying that turbulent transport in the directions normal to gravity is small (or even null). In this case, the Reynolds stresses do not add a 'turbulent' viscosity to the momentum balances because the shear stress is null. Consequently, the mean volume fraction $\langle \alpha_p \rangle$ will be time-dependent in fully developed flows because the 'molecular' viscosity is not large enough to smooth out velocity fluctuations and the compression/expansion of the disperse phase. In short, even a Reynolds-averaged model like the one in Table 2 will exhibit large-scale fluctuations characteristic of single-phase large-eddy simulations [29] if the CIT/BDT forces are large enough.[4] For systems with low mass loading or very dilute systems, there is no mechanism (besides mean shear) to sustain the turbulence in spatially homogeneous flows and thus it will decay in time as seen in single-phase turbulence. Such flows have been widely studied in the literature, and thus are not the target application for the turbulence model described in this work. As shown recently for particle-laden channel flows [30], there is a clear separation between CIT and classical channel flow that occurs for a mass loading near unity. The former lacks 'turbulent' viscosity giving a hyperbolic system, while the latter has strong 'turbulent' viscosity leading to a parabolic system with a time-independent statistics.

[4] For CIT, the mass loading of the particle phase is the key parameter [30], while in BDT the key parameter is $\langle \alpha_p \rangle$ [21].

3.1 Mass

The mass balances in Table 2 use the conserved variables

$$(X_1, X_2, X_3) = (\langle \alpha_p \rangle, \langle \rho_e \alpha_p^\star \rangle, \langle \rho_f \alpha_f^\star \rangle), \tag{9}$$

which are chosen such that the phase-averaged velocities are defined by $\langle \mathbf{u}_p \rangle$ and $\langle \mathbf{u}_f \rangle$. Closures relating (X_1, X_2, X_3) to Reynolds-averaged quantities, e.g., $\langle \rho_f \rangle$, $\langle \alpha_a \rangle$ and $\langle c_m \rangle$, are provided in the table. These formulas simplify significantly when ρ_f can be treated as constant. Because the conserved variables in the mass balances, as well as their fluxes, have the same mathematical form as in the original two-fluid model, the hyperbolicity will not be affected by these choices.

3.2 Momentum

The momentum balances in Table 2 use the conserved variables

$$(X_4, X_5) = (\langle \rho_e \alpha_p^\star \rangle \langle \mathbf{u}_p \rangle, \langle \rho_f \alpha_f^\star \rangle \langle \mathbf{u}_f \rangle), \tag{10}$$

and, hence,

$$(\langle \mathbf{u}_p \rangle_p, \langle \mathbf{u}_f \rangle_f) = \left(\frac{X_4}{X_2}, \frac{X_5}{X_3} \right). \tag{11}$$

The momentum fluxes on the left-hand sides of the momentum balances have an additional contribution due to the phasic Reynolds stresses R_p and R_f. At first glance, one might conclude that the eigenvalues associated with these terms would increase (i.e., the effective pressure increases). However, this is not the case because the total energy is fixed so that increasing R_f results in decreasing $\langle \Theta_f \rangle$ (see definitions of phase-average temperatures in Table 3). Nonetheless, the *effective* particle-phase pressure can increase, especially when the granular temperature is small. In contrast, the closure for $\langle \mathsf{R} \rangle$ can change the eigenvalues. This closure is given in Table 3 and contains a 'laminar' contribution $\langle \mathsf{R}_1 \rangle$ and a turbulent contribution $\langle \mathsf{R}_2 \rangle$. In general, the latter will modify the eigenvalues (e.g., increase their magnitude) due to the difference in turbulence intensities in each phase. Note that the Reynolds-stress tensors are symmetric, positive definite, and therefore the symmetric, non-negative square-root $(\mathsf{R}_f \mathsf{R}_p + \mathsf{R}_p \mathsf{R}_f)^{1/2}$ is uniquely defined using the positive square roots of its (real-valued) eigenvalues.[5] Rescaling this matrix by one-half its trace yields the matrix R_{fp}. In the hyperbolicity analysis, $tr(\langle \mathsf{R} \rangle)$ increases the eigenvalues and $tr(\langle \mathsf{R}_2 \rangle) = 2(k_f^{1/2} - k_p^{1/2})^2$ is non-negative. For the other flux terms, the 'laminar' closures given in Table 3 are retained to ensure that the turbulence model is hyperbolic.

For CIT and BDT, the most important turbulence closure in the momentum balances is the drag modification represented by $(1 - C_d)$ [26]. If the particles remained uniformly distributed in space, then $C_d = 0$; thus, $0 < C_d \leq 1/2$

[5] For CIT and BDT, the Reynolds-stress tensors are diagonal, and hence $\mathsf{R}_f \mathsf{R}_p$ is diagonal and non-negative. However, for mean-shear flows this is not the case, so care must be taken when defining R_{fp} to be sure that the eigenvalues are real-valued.

Table 2. Turbulence model for mean statistics found from two-fluid model in Table 1. The deformation $\langle \mathsf{\Gamma} \rangle$ and strain-rate $\langle \mathsf{S} \rangle$ tensors use the phase-average fluid velocity $\langle \mathbf{u}_f \rangle$. The pressure tensors are defined in Table 3. The Reynolds stresses R_p and R_f and turbulent viscosities $\nu_{p,t}$ and $\nu_{f,t}$ are defined in Table 4.

Mass

$$\begin{aligned}
\partial_t \langle \alpha_p \rangle + \partial_{\mathbf{x}} \cdot (\langle \alpha_p \rangle \langle \mathbf{u}_p \rangle) &= 0 \\
\partial_t \langle \rho_e \alpha_p^\star \rangle + \partial_{\mathbf{x}} \cdot (\langle \rho_e \alpha_p^\star \rangle \langle \mathbf{u}_p \rangle) &= \langle S_a \rangle \\
\partial_t \langle \rho_f \alpha_f^\star \rangle + \partial_{\mathbf{x}} \cdot (\langle \rho_f \alpha_f^\star \rangle \langle \mathbf{u}_f \rangle) &= -\langle S_a \rangle
\end{aligned}$$

Momentum

$$\begin{aligned}
&\partial_t (\langle \rho_e \alpha_p^\star \rangle \langle \mathbf{u}_p \rangle) + \partial_{\mathbf{x}} \cdot (\langle \rho_e \alpha_p^\star \rangle \langle \mathbf{u}_p \rangle \langle \mathbf{u}_p \rangle + \langle \rho_e \alpha_p^\star \rangle \mathsf{R}_p + \langle p_p \rangle \mathsf{I} + \langle \mathsf{P}_{pfp} \rangle) = \\
&(1 - C_d) \langle K \rangle \langle \mathbf{u}_{fp} \rangle - \langle \alpha_p^\star \rangle \partial_{\mathbf{x}} \langle p_f \rangle - \langle \alpha_p^\star \rangle \langle \mathbf{F}_{pf} \rangle + \langle \mathbf{S}_{fp} \rangle + \langle \rho_e \alpha_p^\star \rangle \mathbf{g}
\end{aligned}$$

$$\begin{aligned}
&\partial_t (\langle \rho_f \alpha_f^\star \rangle \langle \mathbf{u}_f \rangle) + \partial_{\mathbf{x}} \cdot (\langle \rho_f \alpha_f^\star \rangle \langle \mathbf{u}_f \rangle \langle \mathbf{u}_f \rangle + \langle \rho_f \alpha_f^\star \rangle \mathsf{R}_f + \langle p_f \rangle \mathsf{I}) = \\
&(1 - C_d) \langle K \rangle \langle \mathbf{u}_{pf} \rangle + \langle \alpha_p^\star \rangle \partial_{\mathbf{x}} \langle p_f \rangle + \langle \alpha_p^\star \rangle \langle \mathbf{F}_{pf} \rangle - \langle \mathbf{S}_{fp} \rangle + \langle \rho_f \alpha_f^\star \rangle \mathbf{g}
\end{aligned}$$

Total Energy

$$\begin{aligned}
&\partial_t (\langle \rho_e \alpha_p^\star \rangle \langle E_p \rangle) + \partial_{\mathbf{x}} \cdot [\langle \rho_e \alpha_p^\star \rangle \langle E_p \rangle \langle \mathbf{u}_p \rangle + \langle \rho_e \alpha_p^\star \rangle \mathsf{R}_p \cdot \langle \mathbf{u}_p \rangle + (\langle p_p \rangle \mathsf{I} + \langle \mathsf{P}_{pfp} \rangle) \cdot \langle \mathbf{u}_p \rangle] = \\
&\partial_{\mathbf{x}} \cdot (\langle \rho_e \alpha_p^\star \rangle \nu_{p,t} \partial_{\mathbf{x}} \langle E_p \rangle) + \langle \mathsf{P}_{pfp} \rangle : \partial_{\mathbf{x}} \langle \mathbf{u}_p \rangle \\
&- \langle K \rangle \left[3 \langle \Theta_p \rangle + 2 k_p - 2 (k_f k_p)^{1/2} + (1 - C_d) \langle \mathbf{u}_p \rangle \cdot \langle \mathbf{u}_{pf} \rangle - C_b \langle u_{fp} \rangle^2 \right] \\
&- \langle \alpha_p^\star \rangle \langle \mathbf{u}_p \rangle \cdot \partial_{\mathbf{x}} \langle p_f \rangle - \langle \alpha_p^\star \rangle \langle \mathbf{u}_p \rangle \cdot \langle \mathbf{F}_{pf} \rangle + \langle S_E \rangle + \langle \rho_e \alpha_p^\star \rangle \langle \mathbf{u}_p \rangle \cdot \mathbf{g}
\end{aligned}$$

$$\begin{aligned}
&\partial_t (\langle \rho_f \alpha_f^\star \rangle \langle E_f \rangle) + \partial_{\mathbf{x}} \cdot [\langle \rho_f \alpha_f^\star \rangle \langle E_f \rangle \langle \mathbf{u}_f \rangle + \langle \rho_f \alpha_f^\star \rangle \mathsf{R}_f \cdot \langle \mathbf{u}_f \rangle + (\langle \alpha_f^\star \rangle \langle \mathbf{u}_f \rangle + \langle \alpha_p^\star \rangle \langle \mathbf{u}_p \rangle) \langle p_f \rangle] = \\
&\partial_{\mathbf{x}} \cdot (\langle \rho_f \alpha_f^\star \rangle \nu_{f,t} \partial_{\mathbf{x}} \langle E_f \rangle) - \langle \mathsf{P}_{pfp} \rangle : \partial_{\mathbf{x}} \langle \mathbf{u}_p \rangle \\
&+ \langle K \rangle \left[3 \langle \Theta_p \rangle + 2 k_p - 2 (k_f k_p)^{1/2} + (1 - C_d) \langle \mathbf{u}_p \rangle \cdot \langle \mathbf{u}_{pf} \rangle - C_b \langle u_{fp} \rangle^2 \right] \\
&+ \langle \alpha_p^\star \rangle \langle \mathbf{u}_p \rangle \cdot \partial_{\mathbf{x}} \langle p_f \rangle + \langle \alpha_p^\star \rangle \langle \mathbf{u}_p \rangle \cdot \langle \mathbf{F}_{pf} \rangle - \langle S_E \rangle + \langle \rho_f \alpha_f^\star \rangle \langle \mathbf{u}_f \rangle \cdot \mathbf{g}
\end{aligned}$$

where

$$\langle \alpha_f \rangle + \langle \alpha_p \rangle = 1 \quad \langle \alpha_f^\star \rangle + \langle \alpha_p^\star \rangle = 1$$

$$\langle \rho_f \alpha_a \rangle = \langle \rho_e \alpha_p^\star \rangle - \rho_p \langle \alpha_p \rangle \quad \langle \rho_f \alpha_f \rangle = \langle \rho_f \alpha_f^\star \rangle + \langle \rho_f \alpha_a \rangle$$

$$\langle \rho_f \rangle = \frac{\langle \rho_f \alpha_f^\star \rangle + \langle \rho_e \alpha_p^\star \rangle - \rho_p \langle \alpha_p \rangle}{\langle \alpha_f \rangle} \quad \langle \alpha_a \rangle = \frac{\langle \rho_e \alpha_p^\star \rangle - \rho_p \langle \alpha_p \rangle}{\langle \rho_f \rangle} \quad \langle c_m \rangle = \frac{\langle \rho_f \alpha_a \rangle}{\langle \rho_f \alpha_f \rangle \langle \alpha_p \rangle}$$

$$\langle K \rangle = \frac{3 \langle \rho_e \alpha_p^\star \rangle C_D Re_p}{4 \tau_p} \quad Re_p = \frac{\langle \alpha_f^\star \rangle}{\langle \alpha_f \rangle} \frac{d_p \langle u_{fp} \rangle}{\nu_f} \quad c_m^\star = \frac{1}{2} \min(1 + 2 \langle \alpha_p \rangle, 2)$$

$$\langle S_a \rangle = \frac{1}{\tau_a} \langle \rho_f \alpha_f \rangle \langle \alpha_p \rangle (c_m^\star - \langle c_m \rangle) \quad \langle \mathbf{S}_{fp} \rangle = \max(\langle S_a \rangle, 0) \langle \mathbf{u}_f \rangle + \min(\langle S_a \rangle, 0) \langle \mathbf{u}_p \rangle$$

$$\langle S_E \rangle = \max(\langle S_a \rangle, 0) \frac{1}{2} \langle u_f \rangle^2 + \min(\langle S_a \rangle, 0) \langle E_p \rangle \quad g_0 = \frac{1 + \langle \alpha_f \rangle}{2 \langle \alpha_f \rangle^3}$$

$$\langle \mathbf{F}_{pf} \rangle = \langle \rho_f \rangle \left[C_c \, tr(\langle \mathsf{\Gamma} \rangle) \mathsf{I} + C_l \langle \mathsf{S} \rangle \right] \cdot \langle \mathbf{u}_{fp} \rangle \quad \langle \mathbf{u}_{pf} \rangle = -\langle \mathbf{u}_{fp} \rangle = \langle \mathbf{u}_p \rangle - \langle \mathbf{u}_f \rangle$$

$$\langle u_{fp} \rangle^2 = \langle \mathbf{u}_{fp} \rangle \cdot \langle \mathbf{u}_{fp} \rangle \quad \langle u_f \rangle^2 = \langle \mathbf{u}_f \rangle_f \cdot \langle \mathbf{u}_f \rangle \quad \langle u_p \rangle^2 = \langle \mathbf{u}_p \rangle \cdot \langle \mathbf{u}_p \rangle$$

Table 3. Pressure tensors for turbulence model in Table 2. Reynolds stresses R_p and R_f are defined in Table 4. All pressure tensors are non-negative and symmetric. $\langle \mathsf{R}_2 \rangle$ is a closure for the turbulent contribution to the pfp-pressure with trace $2(k_f^{1/2} - k_p^{1/2})^2$.

Slip-Velocity Tensor

$$\langle \mathsf{R} \rangle = \langle \mathsf{R}_1 \rangle + \langle \mathsf{R}_2 \rangle$$

$$\langle \mathsf{R}_1 \rangle = \frac{1}{5}\langle u_{fp} \rangle^2 \mathsf{I} + \frac{2}{5}\langle \mathbf{u}_{fp} \rangle \langle \mathbf{u}_{fp} \rangle$$

$$\langle \mathsf{R}_2 \rangle = \frac{2}{5}(k_f^{1/2} - k_p^{1/2})^2 \mathsf{I} + \frac{2}{5}\left(\mathsf{R}_f - 2(k_f k_p)^{1/2} \mathsf{R}_{fp} + \mathsf{R}_p \right)$$

where the symmetric tensor $\mathsf{R}_{fp} = r_{fp}(\mathsf{R}_f \mathsf{R}_p + \mathsf{R}_p \mathsf{R}_f)^{1/2}$ has $tr(\mathsf{R}_{fp}) = 2$, which fixes r_{fp} given the Reynolds-stress tensors.

Particle-Fluid-Particle-Pressure Tensor

$$\langle \mathsf{P}_{pfp} \rangle = C_{pfp} \langle \rho_f \rangle \langle \alpha_p^\star \rangle \langle \mathsf{R} \rangle$$

Fluid Pressure

$$\langle p_f \rangle = \langle \rho_f \rangle (\gamma_f - 1) \langle \Theta_f \rangle - \gamma_f p_f^o$$

Granular Pressure

$$\langle p_p \rangle = \langle \rho_e \alpha_p^\star \rangle \langle \Theta_p \rangle (1 + 4\langle \alpha_p^\star \rangle g_0) + p_c \langle \alpha_p \rangle g_0 \frac{1}{2}\left[1 + \tanh\left(\frac{\langle \alpha_p \rangle - 0.6}{0.01} \right) \right]$$

where

$$\langle \Theta_f \rangle = \langle E_f \rangle - k_f - \frac{1}{2}\langle u_f \rangle^2$$

$$\langle \Theta_p \rangle = \frac{2}{3}\left(\langle E_p \rangle - k_p - \frac{1}{2}\langle u_p \rangle^2 \right)$$

represents reduced drag due to particle clustering. In general, C_d depends on many parameters such as $\langle \alpha_p \rangle$ and Re_p [31]. However, here we simply take $C_d = 0.5$ as the default value, knowing that in most flows it will be smaller. For the other source terms in the momentum balances, most of which affect the hyperbolicity, we use the 'laminar' closure and introduce parameters C_c (compression) and C_l (lift) with default values of unity. These parameters could be fit to canonical cases, for example, involving shocks passing over particle beds (C_c) and mean shear flow (C_l). For the various pressure tensors, use of the 'laminar' forms is justified because they are usually small [18] and will mostly be important for low-turbulent-Reynolds-number flows.

3.3 Total Energy

The total energy balances in Table 2 use the conserved variables

$$(X_6, X_7) = (\langle \rho_e \alpha_p^\star \rangle \langle E_p \rangle, \langle \rho_f \alpha_f^\star \rangle \langle E_f \rangle), \tag{12}$$

and thus

$$(\langle E_p \rangle, \langle E_f \rangle) = \left(\frac{X_6}{X_2}, \frac{X_7}{X_3} \right). \tag{13}$$

The flux closures are analogous to the 'laminar' model but with the additional contribution of the Reynolds stress and the gradient-diffusion model involving turbulent viscosity ν_t (see Table 4). As discussed earlier, one role of the turbulent viscosity is to 'thicken' the shock-like structures that arise due to the high Mach number of the particle phase.

The source terms on the right-hand sides of the energy balances in Table 2 are analogous to the 'laminar' model, but with additional terms that depend on the turbulent kinetic energies (TKE) k_f, k_p and the mean slip velocity $\langle u_{fp} \rangle^2$. Recall that, aside from gravity $\mathbf{g}$, the sum of the source terms for the two phases must be zero due to conservation on energy. Because in most gas–particle flows $k_p < k_f$, the transfer terms move TKE from the particle phase to the fluid phase where it ultimately dissipates to increase $\langle \Theta_f \rangle$. The source terms depending on the mean slip velocity also depend on the material density ratio $Z = \langle \rho_f \rangle / \rho_p$ such that $C_d = C_b + C_g$. As a default closure, we propose the relation given in Table 5, but acknowledge that it is a crude approximation for large Z (i.e., bubbly flows). Physically, C_b corresponds to the particle-phase TKE generated by buoyancy (e.g., BDT) [21], while C_g corresponds to the fluid-phase TKE generated by gravity (e.g., CIT) [26]. In fully developed flow, the terms involving buoyancy and drag are much larger than all of the other source terms. It is interesting to note that the dependence of C_b and C_g on Z implies that in homogeneous bubbly flows $k_f \leq k_p$ [21], while in gas–particle flows $k_p \leq k_f$ [32]. Naturally, for homogeneous suspensions with $Z \approx 1$, $k_p \approx k_f$. Finally, we must remind the reader that the proposed models for C_b and C_g are based on limited data from EE and EL simulations. As is true for C_d, further work is needed to account for the other flow parameters.

3.4 Multiphase Turbulence Statistics

The proposed multiphase turbulence model uses the Reynolds-stress model given in Table 4. By construction, the balances for the Reynolds stresses reduce to those of the TKE, e.g., $2k_f = tr(\mathsf{R}_f)$. The turbulent length and time scales are found using the turbulent dissipate rates (TDR) ε. The models in Table 4 for the TKE and the TDR were first proposed in [26] as generalization of the classical k–ε model [28]. There are two coupling terms, one involving the fluid drag $\langle K \rangle$ and the difference in the statistics in each phase (i.e., the drag-exchange term), and the other is a production term due to the mean-slip velocity. Because the TKE is part of the total energy, the same source terms appear (along with several others) in the total energy balances. Observe that the drag-exchange terms (in isolation) work to equalize the TKE in both phases. On the other hand, the mean-slip-production terms depend on C_b and C_g and inject TKE extracted from the mean kinetic energy. Of these two terms, C_g is important for gas–particle flows, while C_b is important in bubbly flows. At present, only C_g has

been studied in detail [32]. The scaling in terms of Z in the drag-production term involving C_b is unknown, but likely must increase with Z in bubbly flows. Unlike for the total energy of the mixture, the sources terms for TKE of the mixture need not be conservative. In fact, the drag-exchange terms are strictly dissipative for the mixture [26]. At very large mass loading, the magnitudes of the drag-exchange and mean-slip-production terms are much larger than the others and thus determine the values of the TKE and TDR.

The TDR in the TKE balances has the usual form as in single-phase turbulence models, i.e., it dissipates k due to the turbulent energy flux from large to small scales. The constant $C_{\varepsilon,2}$ controls the turbulence decay rate in homogeneous systems [28]. As discussed in [26], the granular temperature equation has the form

$$\begin{aligned}\tfrac{3}{2}\partial_t(\langle\rho_e\alpha_p^\star\rangle\langle\Theta_p\rangle) + \tfrac{3}{2}\partial_{\mathbf{x}}\cdot(\langle\rho_e\alpha_p^\star\rangle\langle\Theta_p\rangle\langle\mathbf{u}_p\rangle) = \tfrac{3}{2}\partial_{\mathbf{x}}\cdot(\langle\rho_e\alpha_p^\star\rangle\nu_{p,t}\partial_{\mathbf{x}}\langle\Theta_p\rangle)\\ -\langle p_p\rangle\partial_{\mathbf{x}}\cdot\langle\mathbf{u}_p\rangle - 3\langle K\rangle\langle\Theta_p\rangle + \langle\rho_e\alpha_p^\star\rangle\varepsilon_p \qquad (14)\end{aligned}$$

where the final term represents production of uncorrelated granular energy due the turbulent dissipation of k_p. Because we use the conservative form of the model with the total energy, this balance equation is not needed. However, one can clearly observed that $\langle\Theta_p\rangle$ is only dissipated by drag (i.e., viscous heating of the fluid). In other words, in the particle phase there is a cascade of energy from large to small scales: $\frac{1}{2}\langle u_p\rangle^2 \to k_p \to \langle\Theta_p\rangle \to \langle\Theta_f\rangle$.

The balance equations for TDR are described in detail in [26]. Again, the two new terms are due to drag exchange and mean-slip production. These terms have the same forms as for the TKE, but there are subtle differences from classical closures used for multiphase turbulence. First, instead of multiplying the drag-exchange term from the TKE by a turbulence time scale, here we define the drag-exchange term using ε (which automatically has the correct units). As shown in [26], by adjusting $C_{\varepsilon,3}$ this simple model reproduces the decay of homogeneous multiphase turbulence in the absence of a mean-slip velocity [11]. The mean-slip-production term uses the timescale τ_p modified by the constant $C_{\varepsilon,4}$. The latter is likely a function of Z and/or mass loading $\varphi = \langle\rho_p\alpha_p\rangle/\langle\rho_f\alpha_f\rangle$. In general, for fixed Z, the value of $C_{\varepsilon,2}/C_{\varepsilon,4}$ controls the magnitude of the steady-state TKE in systems with no production due to mean shear.

Turning now to the balance equations for the Reynolds-stress tensors in Table 4, it is easily verified that their traces reduce to the TKE balances as expected. For the second-order tensors appearing in the balances, the drag-exchange terms are written in terms of the symmetric matrix R_{fp}, defined by rescaling the square-root matrix found from the symmetric form $\mathsf{R}_f\mathsf{R}_p + \mathsf{R}_p\mathsf{R}_f$ such that the trace is equal to two. To the author's knowledge, this simple form has not been used previously and has yet to be tested for flows with mean shear (i.e., away from one-dimensional turbulence). The mean-slip-production terms involve the tensor P_{fp}, which is the dyadic product of the mean-slip velocity. It is this simple (closed) form that leads to diagonal Reynolds stresses for gravity-driven flows in the absence of mean shear. For the other terms, the isotropization tensors Φ have the classical linear form used in single-phase turbulence models

Table 4. Closures for higher-order statistics in the multiphase turbulence model in Table 2. Default values of the model constants are provided in Table 5.

Turbulent Kinetic Energy

$$\partial_t(\langle\rho_f\alpha_f^\star\rangle k_f) + \partial_{\mathbf{x}}\cdot(\langle\rho_f\alpha_f^\star\rangle k_f\langle\mathbf{u}_f\rangle) = \partial_{\mathbf{x}}\cdot(\langle\rho_f\alpha_f^\star\rangle\nu_{f,t}\partial_{\mathbf{x}}k_f) - \langle\rho_f\alpha_f^\star\rangle\varepsilon_f$$
$$-\langle\rho_f\alpha_f^\star\rangle\mathsf{R}_f : \partial_{\mathbf{x}}\langle\mathbf{u}_f\rangle_f + 2\langle K\rangle\left[(k_pk_f)^{1/2} - k_f\right] + C_g\langle K\rangle\langle u_{fp}\rangle^2$$

$$\partial_t(\langle\rho_e\alpha_p^\star\rangle k_p) + \partial_{\mathbf{x}}\cdot(\langle\rho_e\alpha_p^\star\rangle k_p\langle\mathbf{u}_p\rangle) = \partial_{\mathbf{x}}\cdot(\langle\rho_e\alpha_p^\star\rangle\nu_{p,t}\partial_{\mathbf{x}}k_p) - \langle\rho_e\alpha_p^\star\rangle\varepsilon_p$$
$$-\langle\rho_e\alpha_p^\star\rangle\mathsf{R}_p : \partial_{\mathbf{x}}\langle\mathbf{u}_p\rangle + 2\langle K\rangle\left[(k_pk_f)^{1/2} - k_p\right] + C_b\langle K\rangle\langle u_{fp}\rangle^2$$

Turbulent Dissipation Rate

$$\partial_t(\langle\rho_f\alpha_f^\star\rangle\varepsilon_f) + \partial_{\mathbf{x}}\cdot(\langle\rho_f\alpha_f^\star\rangle\varepsilon_f\langle\mathbf{u}_f\rangle) = \partial_{\mathbf{x}}\cdot(\langle\rho_f\alpha_f^\star\rangle\nu_{f,t}\partial_{\mathbf{x}}\varepsilon_f) - C_{\varepsilon,2}\langle\rho_f\alpha_f^\star\rangle\frac{\varepsilon_f}{k_f}\varepsilon_f$$
$$-C_{\varepsilon,1}\frac{\varepsilon_f}{k_f}\langle\rho_f\alpha_f^\star\rangle\mathsf{R}_f : \partial_{\mathbf{x}}\langle\mathbf{u}_f\rangle + 2C_{\varepsilon,3}\langle K\rangle\left[(\varepsilon_p\varepsilon_f)^{1/2} - \varepsilon_f\right] + C_{\varepsilon,4}\frac{1}{\tau_p}C_g\langle K\rangle\langle u_{fp}\rangle^2$$

$$\partial_t(\langle\rho_e\alpha_p^\star\rangle\varepsilon_p) + \partial_{\mathbf{x}}\cdot(\langle\rho_e\alpha_p^\star\rangle\varepsilon_p\langle\mathbf{u}_p\rangle) = \partial_{\mathbf{x}}\cdot(\langle\rho_e\alpha_p^\star\rangle\nu_{p,t}\partial_{\mathbf{x}}\varepsilon_p) - C_{\varepsilon,2}\langle\rho_e\alpha_p^\star\rangle\frac{\varepsilon_p}{k_p}\varepsilon_p$$
$$-C_{\varepsilon,1}\frac{\varepsilon_p}{k_p}\langle\rho_e\alpha_p^\star\rangle\mathsf{R}_p : \partial_{\mathbf{x}}\langle\mathbf{u}_p\rangle + 2C_{\varepsilon,3}\langle K\rangle\left[(\varepsilon_p\varepsilon_f)^{1/2} - \varepsilon_p\right] + C_{\varepsilon,4}\frac{1}{\tau_p}C_b\langle K\rangle\langle u_{fp}\rangle^2$$

Reynolds-Stress Tensor

$$\partial_t(\langle\rho_f\alpha_f^\star\rangle\mathsf{R}_f) + \partial_{\mathbf{x}}\cdot(\langle\rho_f\alpha_f^\star\rangle\langle\mathbf{u}_f\rangle\mathsf{R}_f) = \partial_{\mathbf{x}}\cdot(\langle\rho_f\alpha_f^\star\rangle\nu_{f,t}\partial_{\mathbf{x}}\mathsf{R}_f) - \langle\rho_f\alpha_f^\star\rangle\mathsf{\Phi}_f - \langle\rho_f\alpha_f^\star\rangle\epsilon_f$$
$$+\langle\rho_f\alpha_f^\star\rangle\mathsf{P}_f + 2\langle K\rangle\left((k_fk_p)^{1/2}\mathsf{R}_{fp} - \mathsf{R}_f\right) + 2C_g\langle K\rangle\mathsf{P}_{fp}$$

$$\partial_t(\langle\rho_e\alpha_p^\star\rangle\mathsf{R}_p) + \partial_{\mathbf{x}}\cdot(\langle\rho_e\alpha_p^\star\rangle\langle\mathbf{u}_p\rangle\mathsf{R}_p) = \partial_{\mathbf{x}}\cdot(\langle\rho_e\alpha_p^\star\rangle\nu_{p,t}\partial_{\mathbf{x}}\mathsf{R}_p) - \langle\rho_e\alpha_p^\star\rangle\mathsf{\Phi}_p - \langle\rho_e\alpha_p^\star\rangle\epsilon_p$$
$$+\langle\rho_e\alpha_p^\star\rangle\mathsf{P}_p + 2\langle K\rangle\left((k_fk_p)^{1/2}\mathsf{R}_{fp} - \mathsf{R}_p\right) + 2C_b\langle K\rangle\mathsf{P}_{fp}$$

where $(\mathsf{Y})^\dagger = \frac{1}{2}(\mathsf{Y}+\mathsf{Y}^t)$, $\mathsf{R}_{fp} \propto (\mathsf{R}_f\mathsf{R}_p + \mathsf{R}_p\mathsf{R}_f)^{1/2}$ with $tr(\mathsf{R}_{fp}) = 2$,

$$\tau_p = \frac{\langle\rho_e\alpha_p^\star\rangle}{\langle K\rangle} \qquad \nu_{f,t} = C_{\mu,f}\frac{k_f^2}{\varepsilon_f} \quad \nu_{p,t} = C_{\mu,p}\frac{k_p^2}{\varepsilon_p} \qquad \mathsf{P}_{fp} = \langle\mathbf{u}_{fp}\rangle\langle\mathbf{u}_{fp}\rangle \quad P_{fp} = tr(\mathsf{P}_{fp})$$

$$\mathsf{P}_f = -2(\mathsf{R}_f\cdot\partial_{\mathbf{x}}\langle\mathbf{u}_f\rangle)^\dagger \quad P_f = tr(\mathsf{P}_f) \qquad \mathsf{P}_p = -2(\mathsf{R}_p\cdot\partial_{\mathbf{x}}\langle\mathbf{u}_p\rangle)^\dagger \quad P_p = tr(\mathsf{P}_p)$$
$$\mathsf{\Phi}_f = C_{1f}\frac{\varepsilon_f}{k_f}\left(\mathsf{R}_f - \frac{2}{3}k_f\mathsf{I}\right) + C_{2f}\left(\mathsf{P}_f - \frac{1}{3}P_f\mathsf{I}\right) + C_{fp}\frac{2C_g\langle K\rangle}{\langle\rho_f\alpha_f^\star\rangle}\left(\mathsf{P}_{fp} - \frac{1}{3}P_{fp}\mathsf{I}\right)$$
$$\mathsf{\Phi}_p = C_{1p}\frac{\varepsilon_p}{k_p}\left(\mathsf{R}_p - \frac{2}{3}k_p\mathsf{I}\right) + C_{2p}\left(\mathsf{P}_p - \frac{1}{3}P_p\mathsf{I}\right) + C_{fp}\frac{2C_b\langle K\rangle}{\langle\rho_e\alpha_p^\star\rangle}\left(\mathsf{P}_{fp} - \frac{1}{3}P_{fp}\mathsf{I}\right)$$
$$\epsilon_f = \left(C_f\frac{1}{k_f}\mathsf{R}_f + \frac{2}{3}(1-C_f)\mathsf{I}\right)\varepsilon_f \qquad \epsilon_p = \left(C_p\frac{1}{k_p}\mathsf{R}_p + \frac{2}{3}(1-C_p)\mathsf{I}\right)\varepsilon_p$$

Table 5. Default values of the turbulence model constants with $Z = \langle \rho_f \rangle / \rho_p$. For water, $\gamma_f = 6.1$ and $p_f^o = 4 \times 10^8$ Pa. For air, $\gamma_f = 1.4$ and $p_f^o = 0$ Pa. Except perhaps for $Z \leq 1$, the expressions for C_g and C_b are rough approximations and should not be used for $1 \ll Z$ (where $C_g \approx 0$) as explained in the main text. More generally, the dissipation model parameters must be fit to data for statistically homogeneous flows, especially for large Z (bubbly flows).

Constant	Value
c_f	0.2
C_c	1
C_l	1
C_g	$[\langle \alpha_f \rangle - \langle \alpha_a \rangle \min(Z, 1)] C_d$
C_b	$[\langle \alpha_p \rangle + \langle \alpha_a \rangle \min(Z, 1)] C_d$
C_d	0.5
$C_{\mu,f}$, $C_{\mu,f}$	0.09
C_{1f}	1.5
C_{1p}	1.5
C_{2f}	0.6
C_{2p}	0.6
C_{fp}	0
C_f, C_p	0
$C_{\varepsilon,1}$	1.44
$C_{\varepsilon,2}$	1.92
$C_{\varepsilon,3}$	1.92
$C_{\varepsilon,4}$	1.92

[28], and the Rotta model is used for the turbulent dissipation tensors ϵ. Obviously, other forms of these terms are possible, and likely desirable, to capture the temporal and spatial variations of the Reynolds stresses in real disperse multiphase flows.

Finally, we should note that in the hyperbolicity analysis the eigenvalues associated with the TKE and TDR balances are just the mean velocities. Thus, the hyperbolicity of the turbulence model is not compromised. Nonetheless, as mentioned earlier in the discussion of Table 2, the magnitude of some of the eigenvalues will increase with increasing TKE. In other words, the speed of some processes will become faster when turbulence is present. However, the largest eigenvalues (which control the numerical time step [18]) are usually fixed by the speed of sound in the fluid ($\sqrt{\gamma_f p_f^o}$). If the fluid phase were treated as incompressible [18], then the speed of sound for the particle phase (which depends on $\sqrt{6k_p}$) would determine the time step.

3.5 Summary

In addition to the seven conserved variables X_i corresponding to the mean statistics, the turbulence model introduces four additional conserved quantities:

$$(X_8, X_9, X_{10}, X_{11}) = (\langle \rho_e \alpha_p^\star \rangle \mathsf{R}_p, \langle \rho_f \alpha_f^\star \rangle \mathsf{R}_f, \langle \rho_e \alpha_p^\star \rangle \varepsilon_p, \langle \rho_f \alpha_f^\star \rangle \varepsilon_f). \quad (15)$$

The Reynolds stresses contain six variables each; however, in homogeneous CIT and BDT, only two of the six are independent. The default values for the model constants are provided in Table 5. Nonetheless, further research is needed to determine whether (1) the simple linear-relaxation model used for the Reynolds stresses is sufficient to handle a wide range of flows, (2) whether the default values of the constants need to be adjusted or made to depend on flow parameters such as Re_p and $\langle \alpha_p \rangle$, and (3) what additional terms beyond the 'laminar' terms are needed in the flux and source-term closures.

Finally, we should remind the reader that the starting two-fluid model in Table 1 neglects viscous stresses in the fluid phase, assumes elastic collisions for the particles, and treats all particles as adiabatic spheres with identical properties. While all of these additional effects can easily be included in the turbulence model, at present the model in Table 2 is applicable only to high-turbulent-Reynolds-number flows. For many applications, the main effect of the turbulence model will be to modify the phasic speeds of sound due to the TKE. For example, gas–particle flows with $Z = 0$ and negligible granular temperature have a particle-phase speed of sound equal to $\sqrt{6k_p}$. In principle, if k_p were large enough to make the particle phase subsonic, then a much coarser grid could be employed to resolve the particle phase.

Another important consideration when applying the turbulence model to real flows are the boundary conditions. For example, in particle-laden channel flows with significant mass loading the fluid-phase turbulence structures are altered by the presence of the clusters, which changes the behavior of the turbulent boundary layer [17,30]. Although some initial work on developing boundary conditions for channel flows has been reported [33], much work remains to accommodate more general flow geometries. Thus, in the example applications below, we will focus on homogeneous systems for which boundary conditions are not required.

4 Application to Statistically Homogeneous Flows

As an example application, we consider statistically homogeneous flows that are controlled by the drag-exchange and mean-slip-production terms. Two specific examples of such flows are (i) cluster-induced turbulence with $Z \approx 0$ [20] and (ii) buoyancy-driven turbulence with $1 \ll Z$ [21].

4.1 Mass Balances

For statistically stationary and spatially homogeneous flows, the turbulence model reduces to algebraic relations. For example, $\langle \alpha_p \rangle$ is a fixed constant, so

that $\langle c_m \rangle = c_m^\star = \frac{1}{2} + \langle \alpha_p \rangle$ and $\langle \alpha_a \rangle = \langle c_m \rangle \langle \alpha_p \rangle \langle \alpha_f \rangle$ are constants. Furthermore, compressibility plays no role in these flows, so that ρ_f is constant and

$$\frac{\langle \rho_f \alpha_f^\star \rangle}{\langle \rho_e \alpha_p^\star \rangle} = \frac{Z \langle \alpha_f^\star \rangle}{\langle \alpha_p \rangle + Z \langle \alpha_a \rangle} \tag{16}$$

where $Z = \rho_f / \rho_p$ and the second term in the denominator is the contribution due to added mass. In general, any averaged variable involving the volume fractions and/or densities is time independent for spatially homogeneous flows.

4.2 Momentum Balances

The mean-slip velocity $\langle \mathbf{u}_{fp} \rangle$ is with respect to the *bulk* fluid velocity $\langle \mathbf{u}_f \rangle$ and not the fluid velocity $\langle \mathbf{v}_f \rangle$. As shown in [18], they differ by a factor of $\langle \alpha_f \rangle / \langle \alpha_f^\star \rangle$, i.e., $\langle \alpha_f^\star \rangle \langle \mathbf{u}_{pf} \rangle = \langle \alpha_f \rangle \langle \mathbf{v}_{pf} \rangle$. In most simulations of statistically homogeneous flows, $\langle \mathbf{v}_f \rangle$ is set to zero by controlling the fluid pressure gradient. For the fluid velocity to be null, we must have $\langle \rho_f \alpha_f^\star \rangle \langle \mathbf{u}_f \rangle = -\langle \rho_f \alpha_a \rangle \langle \mathbf{u}_p \rangle$, i.e., the bulk fluid velocity is opposite the particle velocity and proportional to the added mass. The mean-slip velocity is related to the mean particle velocity by

$$\langle \mathbf{u}_{pf} \rangle = \frac{\langle \alpha_f \rangle}{\langle \alpha_f^\star \rangle} \langle \mathbf{u}_p \rangle. \tag{17}$$

Thus, $\langle \alpha_f^\star \rangle d\langle \mathbf{u}_{pf} \rangle / dt = \langle \alpha_f \rangle d\langle \mathbf{u}_p \rangle / dt$ for statistically homogeneous flows.

We can take gravity to be $\mathbf{g} = g(t)\mathbf{e}_x$ where $g(t)$ is a possibly time-dependent magnitude. From the mixture momentum balance, we then find

$$\partial_{\mathbf{x}} \langle p_f \rangle + \rho_p \langle \alpha_p \rangle \partial_t \langle \mathbf{u}_p \rangle = (\rho_p \langle \alpha_p \rangle + \rho_f \langle \alpha_f \rangle) g(t) \mathbf{e}_x. \tag{18}$$

The mean-slip velocity is then set by $\langle \mathbf{u}_{pf} \rangle = \langle u_{pf} \rangle \mathbf{e}_x$, which is determined from the balance between gravity, buoyancy and fluid drag. Using (18) to eliminate the fluid-phase pressure gradient, the particle-phase momentum balance reduces to

$$\frac{\rho_p \langle \alpha_p \rangle \langle \alpha_f^\star \rangle + \rho_f \langle \alpha_a \rangle}{\langle K \rangle} \frac{d\langle u_p \rangle}{dt} = -(1 - C_d) \langle u_{pf} \rangle + \frac{\langle \alpha_f^\star \rangle \rho_p \langle \alpha_p \rangle (1 - Z)}{\langle K \rangle} g(t). \tag{19}$$

For a steady-state system, $g(t) = g$ is constant. With Stokes drag, $\langle K \rangle$ is

$$\langle K \rangle = \langle \rho_e \alpha_p^\star \rangle \frac{18 \mu_f}{\rho_p d_p^2} = \langle \rho_e \alpha_p^\star \rangle \frac{1}{\tau_p} \tag{20}$$

and the mean-slip velocity is

$$\langle u_{pf} \rangle = \frac{\langle \alpha_f^\star \rangle (1 - Z) \tau_p g}{(1 - C_d)(1 + Z \langle c_m \rangle \langle \alpha_f \rangle)}. \tag{21}$$

For CIT, $Z \approx 0$ so that $\langle u_{pf} \rangle$ has the same direction as gravity. The opposite is observed with BDT.

Recall that the factor $(1 - C_d)$ accounts for clustering, i.e., the magnitude of the mean-slip velocity increases compared to uniform flows. In the very dilute limit ($\langle \alpha_p \rangle \to 0$) there are no clusters, so that the mean-slip velocity for Stokes flow is

$$\langle u_{pf} \rangle_0 = \frac{1 - Z}{1 + Z\langle c_m \rangle} \tau_p g. \tag{22}$$

For finite Re_p, the drag coefficient will depend on Re_p and the volume fraction. Nevertheless, the mean-slip velocity is uniquely determined from (19). By defining $\tau_p^\star$ as

$$\tau_p^\star = \frac{\langle \rho_e \alpha_p^\star \rangle}{\langle K \rangle}, \tag{23}$$

the terminal velocity $V_t = \tau_p^\star g |1 - Z|/(1 + Z\langle c_m \rangle)$ is defined for arbitrary Re_p.

4.3 Granular Energy Balance

The total energy equation for the fluid provides no new information. For the particle phase, the steady-state granular temperature is found from (14):

$$\langle \Theta_p \rangle = \frac{\langle \rho_e \alpha_p^\star \rangle}{3\langle K \rangle} \varepsilon_p = \frac{1}{3} \tau_p^\star \varepsilon_p, \tag{24}$$

and thus depends on the value of $\tau_p^\star \varepsilon_p$. In the model for CIT and BDT, the granular temperature does not affect any of the other variables. However, direct-numerical simulations of uniform systems suggest that it may modify the drag coefficient C_D [34]. At least for CIT, the amount of total energy represented by $\langle \Theta_p \rangle$ is relatively small as compared to k_p (i.e., approximately 10% of the turbulent kinetic energy [32]).

4.4 Turbulent Kinetic Energy Balances

The TKE and TDR are found by solving four differential equations:[6]

$$\frac{\rho_f \langle \alpha_f^\star \rangle}{\langle \rho_e \alpha_p^\star \rangle} \frac{d\hat{k}_f}{d\hat{t}} = 2(\hat{k}_p \hat{k}_f)^{1/2} - 2\hat{k}_f + \hat{C}_g \gamma(\hat{t}) - \frac{\rho_f \langle \alpha_f^\star \rangle}{\langle \rho_e \alpha_p^\star \rangle} \hat{\varepsilon}_f, \tag{25}$$

$$\frac{d\hat{k}_p}{d\hat{t}} = 2(\hat{k}_p \hat{k}_f)^{1/2} - 2\hat{k}_p + \hat{C}_b \gamma(\hat{t}) - \hat{\varepsilon}_p, \tag{26}$$

$$\frac{\rho_f \langle \alpha_f^\star \rangle}{\langle \rho_e \alpha_p^\star \rangle} \frac{d\hat{\varepsilon}_f}{d\hat{t}} = 2C_{\varepsilon,3}[(\hat{\varepsilon}_p \hat{\varepsilon}_f)^{1/2} - \hat{\varepsilon}_f] + C_{\varepsilon,4} \hat{C}_g \gamma(\hat{t}) - \frac{\rho_f \langle \alpha_f^\star \rangle}{\langle \rho_e \alpha_p^\star \rangle} C_{\varepsilon,2} \hat{\omega}_f \hat{\varepsilon}_f, \tag{27}$$

[6] Only algebraic equations are required at steady state, but the differential equations provide information concerning the stability and relaxation behavior of the solution.

$$\frac{d\hat{\varepsilon}_p}{d\hat{t}} = 2C_{\varepsilon,3}[(\hat{\varepsilon}_p\hat{\varepsilon}_f)^{1/2} - \hat{\varepsilon}_p] + C_{\varepsilon,4}\hat{C}_b\gamma(\hat{t}) - C_{\varepsilon,2}\hat{\omega}_p\hat{\varepsilon}_p \tag{28}$$

where $\hat{C}_g = C_g/C_d$ and $\hat{C}_b = C_b/C_d$ (which are non-negative, depend on Z, and sum to unity) modify the split of the TKE between the phases. The dimensionless variables are defined by

$$\hat{t} = \frac{t}{\tau_p^\star}, \quad \hat{k} = \frac{k}{C_d V_t^2}, \quad \hat{\varepsilon} = \frac{\tau_p^\star \varepsilon}{C_d V_t^2}, \quad \hat{\omega} = \frac{\hat{\varepsilon}}{\hat{k}}, \quad \gamma(\hat{t}) = \frac{\langle u_{pf}\rangle^2}{V_t^2} \tag{29}$$

where $\tau_p^\star$ is defined by (23). The forcing term $\gamma(\hat{t})$ is constant at steady state, but can be made to vary with time by making $g(t)$ time dependent in (19), e.g., with periodic forcing $g(t) = g\cos(\omega_g\hat{t})$.

The steady-state solution depends on the parameter ratios $R_3 = C_{\varepsilon,3}/C_{\varepsilon,2}$ and $R_4 = C_{\varepsilon,4}/C_{\varepsilon,2}$. In general, if $R_3 = 1$ then the steady-state solution gives $\hat{\omega}_p = \hat{\omega}_f$, and hence $\hat{\varepsilon}_f = \hat{\omega}\hat{k}_f$ and $\hat{\varepsilon}_p = \hat{\omega}\hat{k}_p$ where $\hat{\omega} = R_4$ is the shared frequency. Then, for $Z = 1$, if $\hat{C}_g(1) = \langle\alpha_f^\star\rangle$ and $\hat{C}_b(1) = \langle\alpha_p^\star\rangle$, the steady-state solution will be $\hat{k}_f = \hat{k}_p = 1/R_4$. In general, C_d is used to control the mean-slip velocity, thus the magnitude of the TKE can controlled using R_4.[7] Then the TKE ratio $R_{TKE} = \hat{k}_f/\hat{k}_p$ for other values of Z is controlled by the model for $\hat{C}_g(Z)$ (given that $\hat{C}_b(Z) = 1 - \hat{C}_g(Z)$). For example, for $1 \ll Z$ it is known that $R_{TKE} < 1$ but nearly constant for fixed $\langle\alpha_p\rangle$, e.g., $R_{TKE} \approx 0.696$ for $\langle\alpha_p\rangle = 0.5$ and $Z = 1000$ [21]. On the other hand, for $Z \approx 0$, $R_{TKE} > 1$, e.g., $R_{TKE} \approx 1.66$ for $\langle\alpha_p\rangle = 0.01$ and $Z = 0.001$ [32].

In summary, the default dissipation parameters are $C_{\varepsilon,3} = C_{\varepsilon,2} = 1.92$ and $C_{\varepsilon,4} = R_4 C_{\varepsilon,2}$ where R_4 can be set to control the level of the TKE. The parameters $C_b(Z)$ and $C_g(Z)$ have the property $C_b + C_g = C_d$ where C_d fixes the mean-slip velocity and depends on Z, Re_p and $\langle\alpha_p\rangle$. The ratio $\hat{C}_g(Z)$ must have the properties $\hat{C}_g(1) = \langle\alpha_f^\star\rangle$ and $\hat{C}_g(0) = 1$. For other values of Z, $\hat{C}_g(Z)$ is chosen to fix the TKE ratio R_{TKE}, but must always be non-negative and less than unity. Also, for simplicity, the drag-exchange term for TKE and TDR is written here with the correlation constants βk and β_ε (see [26]) equal to one. At least for CIT with $\hat{C}_g = 1$, other values may be needed for these parameters to get the correct R_{TKE}. As in other dynamical systems, it would be informative to compare the model to Euler–Lagrange or two-fluid simulations with periodic forcing, i.e., $g(t) = g\cos(\omega_g\hat{t})$, for different values of the forcing frequency ω_g. For a given Z, the dynamical response of R_{TKE} would provide valuable information concerning R_3 and R_4 that is indiscernible from the steady-state solution.

[7] Adjusting R_4 is physically equivalent to adjusting the timescale for the cluster-induced turbulence relative to τ_p as defined in (23). For bubbly flow with $1 \ll Z$ the predicted value of k_f is very small when $R_4 = 1$. However, since part of the fluid travels with the particles, k_f is less than the TKE of fluid reported in [21].

4.5 Reynolds Stresses

Turning now to the Reynolds stresses, in the coordinate system with the x-axis aligned opposite of $\mathbf{g}$ (i.e., $\mathbf{e}_x \cdot \mathbf{g} = -g$), the stress tensor will be diagonal with $R^\star_{xx} > R^\star_{yy} = R^\star_{zz}$. Thus, for each phase there are only two independent components and $2k^\star = R^\star_{xx} + 2R^\star_{yy}$. The mean-slip-production tensor P_{fp} has only the xx-component nonzero and is equal to $\langle u_{fp}\rangle^2$. The dimensionless isotropization tensors are traceless and have the form

$$\hat{\Phi}_f = 2C_{1f}\hat{\varepsilon}_f\left(\tilde{\mathsf{R}}_f - \frac{1}{3}\mathsf{I}\right) + 2C_{fp}\hat{C}_g\gamma(\hat{t})\frac{\langle\rho_e\alpha_p^\star\rangle}{\rho_f\langle\alpha_f^\star\rangle}\left(\mathbf{e}_x\mathbf{e}_x - \frac{1}{3}\mathsf{I}\right) \tag{30}$$

$$\hat{\Phi}_p = 2C_{1p}\hat{\varepsilon_p}\left(\tilde{\mathsf{R}}_p - \frac{1}{3}\mathsf{I}\right) + 2C_{fp}\hat{C}_b\gamma(\hat{t})\left(\mathbf{e}_x\mathbf{e}_x - \frac{1}{3}\mathsf{I}\right) \tag{31}$$

where $\tilde{\mathsf{R}} = \mathsf{R}^\star/(2k^\star)$ is diagonal with unit trace. The first term reorients TKE from the xx-component towards the other diagonal components, while the second term makes the mean-slip-production term more isotropic. The dimensionless dissipation tensors are

$$\hat{\epsilon}_f = 2\left(C_f\tilde{\mathsf{R}}_f + \frac{1}{3}(1-C_f)\mathsf{I}\right)\hat{\varepsilon}_f \quad \hat{\epsilon}_p = 2\left(C_p\tilde{\mathsf{R}}_p + \frac{1}{3}(1-C_p)\mathsf{I}\right)\hat{\varepsilon}_p \tag{32}$$

where $tr(\hat{\epsilon}) = 2\hat{\varepsilon}$. As in single-phase turbulence, the term involving C_f (C_p) in (32) can be combined with the C_1 term in Φ, hence we can let $C_f = C_p = 0$.[8]

With these definitions, the Reynolds stresses are found from

$$\frac{\rho_f\langle\alpha_f^\star\rangle}{\langle\rho_e\alpha_p^\star\rangle}\frac{d\hat{\mathsf{R}}_f}{d\hat{t}} = 2(\hat{k}_f\hat{k}_p)^{1/2}\mathsf{R}_{fp} - 2\hat{\mathsf{R}}_f + 2\hat{C}_g\gamma(\hat{t})\mathbf{e}_x\mathbf{e}_x - \frac{\rho_f\langle\alpha_f^\star\rangle}{\langle\rho_e\alpha_p^\star\rangle}(\hat{\Phi}_f + \hat{\epsilon}_f) \tag{33}$$

$$\frac{d\hat{\mathsf{R}}_p}{d\hat{t}} = 2(\hat{k}_f\hat{k}_p)^{1/2}\mathsf{R}_{fp} - 2\hat{\mathsf{R}}_p + 2\hat{C}_b\gamma(\hat{t})\mathbf{e}_x\mathbf{e}_x - (\hat{\Phi}_p + \hat{\epsilon}_p) \tag{34}$$

where $tr(\hat{\mathsf{R}}) = 2\hat{k}$ and R_{fp} is defined such that $tr(\mathsf{R}_{fp}) = 2$:

$$\mathsf{R}_{fp} = 2(\tilde{R}_{xx}^{1/2} + 2\tilde{R}_{yy}^{1/2})^{-1}diag(\tilde{R}_{xx}^{1/2}, \tilde{R}_{yy}^{1/2}, \tilde{R}_{yy}^{1/2}), \tag{35}$$

and $\tilde{R}_{xx}$, $\tilde{R}_{yy}$ are the two independent components of the diagonal matrix $\tilde{\mathsf{R}}_f\tilde{\mathsf{R}}_p$. Given the solution for the TKE and TDR, the xx-component of the relations in (33) and (34) can be solved to find $\hat{R}_{xx}$ for each phase. Note that the drag-exchange terms couple the two phases and work to equalize the anisotropy between phases. In contrast, the mean-slip-production term is highly anisotropic and would drive the system to $\tilde{R}_{xx} = 1$ if not for the isotropization term $\hat{\Phi}$. For example, with $C_{fp} = 1$ the production terms will be isotropic so that $\tilde{R}_{xx} = 1/3$.

[8] For particle-laden flows, the particle-pressure tensor is highly anisotropic [35]. In general, if a full second-order model is used for the particle phase [36], nonzero C_p is required to predict this anisotropy [32].

For the isotropization term, one can first set C_1 to the standard value for single-phase turbulence [28], and then use $0 \leq C_{fp} < 1$ to achieve the correct value for $\tilde{R}_{zz}$. This statement assumes that with $C_{fp} = 0$, $\tilde{R}_{xx}$ is too large when the standard value of C_1 is used. If this is not the case, then C_1 must be decreased to get the desired value for $\hat{R}_{xx}$.

Table 6. Steady-state predictions from the turbulence model with default values of parameters in Table 5. The particle volume fractions are chosen to correspond to CIT [32] and BDT [21]. The statistics $\tilde{R}$ are the xx component of the Reynolds-stress tensor scaled by $2\hat{k}$. For the default parameters $\hat{\varepsilon} = \hat{k}$ and dimensionless mean-slip velocity is unity.

Z	$\langle\alpha_p\rangle$	$\hat{k}_f$	$\hat{k}_p$	R_{TKE}	$\tilde{R}_f$	$\tilde{R}_p$
0.001	0.01	1.307	0.588	2.223	0.871	0.750
1	0.1	0.154	0.154	1	0.778	0.778
1000	0.5	0.403	0.569	0.708	0.752	0.797
1000	0.1	0.057	0.102	0.559	0.774	0.818

4.6 Example Results

To show predictions from the multiphase turbulence model, we will use the default parameters and three values for Z, namely, 0.001, 1, and 1000. The first corresponds to gas–particle flow, the second to buoyancy-neutral flow, and the third to bubbly flow. For the default parameters, the steady-state frequencies are $\hat{\omega}_p = \hat{\omega}_f = 1$. Steady-state results for the other statistics are given in Table 6. As expected, for $Z = 1$ both phases have the same values for all statistics. We should mention that for $Z = 1$, we find $V_t = 0$ so that the dimensional statistics are null. As expected, for gas–particle flow $\hat{k}_f \gg \hat{k}_p$ and $\tilde{R}_f$ is near 0.9 [32]. However, R_{TKE} is larger than observed in [32]. Likewise, for bubbly flow $\hat{k}_f < \hat{k}_p$ [21]. Here, R_{TKE} for $\langle\alpha_p\rangle = 0.5$ is close to the value observed in [21]. These trends validate the structure of the mathematical model and its dependence on Z. Quantitative agreement with direct-simulation data can be obtained by optimizing the parameters around their default values in Table 5. For bubbly flow, no turbulence is observed for $\langle\alpha_p\rangle \leq 0.3$ in direct simulations [21]. The turbulence model predicts a much lower, but nonzero, value for the dimensionless TKE. However, recall that $C_d = 0$ when the flow is non-turbulent (i.e., when only pseudoturbulence present [37]) and, hence, the dimensional TKE $k^\star$ will be null. In other words, the transition to turbulence must be incorporated into the drag closure for C_d.

An example of the time-dependent turbulence model predictions for gas–particle flow with periodic forcing $g(\hat{t}) = \cos(\omega_g \hat{t})$ and $\omega_g = \pi/3$ is shown in Fig. 1. In the top panel, u_p is scaled such that the steady-state value is unity. At the chosen frequency, the mean-slip velocity lags behind the forcing and has

maximum magnitude of approximately 0.5. In the second panel, as expected, the TKE oscillates at twice the frequency of $g(\hat{t})$ and its magnitude is significantly lower than the steady-state value in Table 6. In the third panel, the TKE and TDR ratios are seen to vary significantly with time, as is the case for $\hat{\omega}$ in the bottom panel. It is noteworthy that the phasic $\hat{\omega}$ are not equal, and most of the time are below the steady-state value of unity. These differences are due to the fact that the characteristic timescale for the fluid from (16) depends on the value of Z. The results for $Z \gg 1$ follow similar trends to those in Fig. 1. From the point of view of fitting the model parameters, the periodic-forcing data are much richer than the steady-state data. It would therefore be useful to obtain such data from direct simulations for model validation. Finally, we can note that the dissipation parameter $C_{\varepsilon,2}$ can be fit to direct-simulation data by starting from steady state and observing the decay rate of $\hat{\varepsilon}$ with $g = 0$.

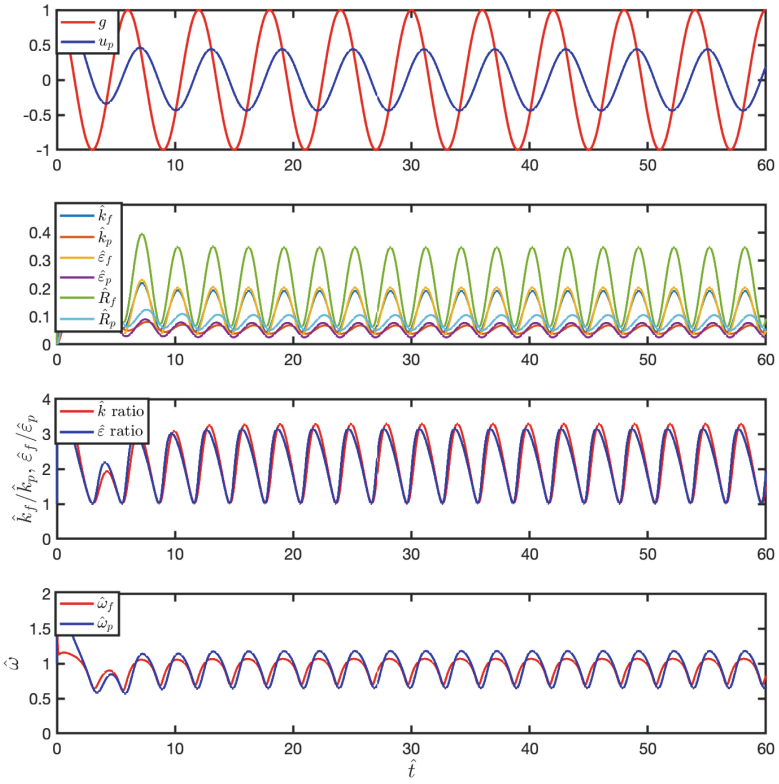

Fig. 1. Example predictions from multiphase turbulence model for CIT with $Z = 0.001$, $\langle \alpha_p \rangle = 0.01$, $\omega_g = \pi/3$, and default parameters in Table 5. All model variables are dimensionless and R_f and R_p are the xx-component of the Reynolds stresses. **top** $g(\hat{t})$ and $u_p(\hat{t})$. **middle-top** $\hat{k}_f(\hat{t})$, $\hat{k}_p(\hat{t})$, $\hat{\varepsilon}_f(\hat{t})$, $\hat{\varepsilon}_p(\hat{t})$, $\hat{R}_f(\hat{t})$, $\hat{R}_p(\hat{t})$. **middle-bottom** $R_{TKE}(\hat{t})$, $R_{TDR}(\hat{t})$. **bottom** $\hat{\omega}_f(\hat{t})$, $\hat{\omega}_p(\hat{t})$

5 Conclusions

Starting from a hyperbolic two-fluid model for monodisperse multiphase flow consisting of a compressible fluid and incompressible spherical particles, a multiphase turbulence model is proposed based on Reynolds averaging. In order to allow for arbitrary material-density ratios, the two-fluid model includes the added mass due to the fluid in particle wakes, which travels with the velocity of the particles. The fluid phase is thus divided into a bulk fluid and the added mass, which travel at different velocities. As shown in previous work [18], this two-fluid formulation involving seven equations is globally hyperbolic. By carefully formulating the closures in the turbulence model, the latter retains the same hyperbolicity characteristics as the original two-fluid model. However, the phasic speeds of sound are altered due to the 'turbulent pressure' associated with the phasic turbulent kinetic energies.

In addition to the seven conserved variables, the turbulence model includes four additional balance equations for the fluid- and particle-phase Reynolds stresses and turbulence dissipation rates. In the target application—gravity-driven turbulence—the Reynolds-stress tensors are diagonal but anisotropic. Thus, they do not produce 'turbulent-viscosity' terms in the mean momentum balances as in classical mean-shear flows. For this reason, the characteristic timescales in the hyperbolic multiphase turbulence model are similar to the original two-fluid model (albeit with a higher speed of sound due to the turbulent kinetic energy), and solutions to the multiphase turbulence model for real applications—such as particle-laden riser flow—will not be time independent. Nonetheless, 'turbulent diffusion' of turbulent kinetic energy and its dissipation will be present. Together with the higher speed of sound in the particle phase, this should make it possible to achieve accurate time-dependent solutions on coarser grids than would be the case with the original two-fluid model.

The closures employed in the balances for turbulent kinetic energy were, for the most part, originally proposed in [26]. Both drag and mean-shear production are included in these balances, and the form of the drag-exchange term has been discussed in detail in [26]. The balances for the turbulent dissipation rates follow the same formulation, but we have introduced a slight (but important) change in the drag-production term. Contrary to what was done in [26], the characteristic timescale for drag production in the dissipation equation is τ_p. This change was made to allow for stationary solutions for homogeneous gravity-driven turbulence, and is consistent with the treatment of pseudoturbulence in [18]. We have also shown that the dissipation parameters must be made to depend on Z (i.e., the material-density ratio) in order to reproduce the behavior seen in CIT and BDT (and the anticipated equality of the turbulence statistics for $Z = 1$). Nevertheless, further work is needed to determine how these parameters depend on the other properties of the flow (e.g., mass loading, particle Reynolds number, etc.).

For the Reynolds-stress balances, the closures for the isotropization tensors are the simplest linear-relaxation models from the literature. This choice was made because data are lacking to validate more complex closures involving non-

linear terms. The proposed closures for the drag-exchange terms for the Reynolds stresses are novel. First, their trace yields the correct expression for the drag-exchange model for the turbulent kinetic energies. Second, their mathematical forms are analogous to the latter (e.g., linear terms keep the same form but replace the scalar with the tensor). Thus, the most speculative closure is the tensor R_{fp} towards which the phasic Reynolds stresses relax due to drag coupling. Obviously, this tensor is not unique, but its form (e.g., symmetric, positive-definite) can be tested for gravity-driven and mean-shear flows in future work.

In summary, we have presented a 'basic' multiphase turbulence model for compressible disperse multiphase flows. This model has favorable mathematical properties (e.g., hyperbolic, realizable, etc.) that will make its numerical implementation in compressible flow codes very robust. Future work will be devoted to validating the closures and extending them as needed to account for multiphase turbulence physics in systems with both gravity-driven and mean-shear turbulence production.

References

1. Theofanous, T.G., Sullivan, J.: J. Fluid Mech. **116**, 343 (1982)
2. Besnard, D.C., Harlow, F.H.: Int. J. Multiphase Flow **14**(6), 679 (1988)
3. Champney, J.M., Dobrovolskis, A.R., Cuzzi, J.N.: Phys. Fluids **7**(7), 1703 (1995)
4. Bi, H.T., Ellis, N., Abba, I.A., Grace, J.R.: Chem. Eng. Sci. **55**, 4789 (2000)
5. Sundaresan, S.: AIChE J. **46**(6), 1102 (2000)
6. Krause, M.: New Astron. Rev. **51**, 174 (2007)
7. Doronzo, D.M., de Tullio, M.D., Pascazio, G.: Comput. Fluids **44**, 56 (2011)
8. Colombo, M., Fairweather, M.: Int. J. Multiphase Flow **77**, 222 (2015)
9. Besagni, G., Guédon, G.R., Inzoli, F.: Nucl. Eng. Des. **331**, 222 (2018)
10. Sun, Z., Zhu, J.: AIChE J. **65**(9), 1 (2019)
11. Février, P., Simonin, O., Squires, K.D.: J. Fluid Mech. **533**, 1 (2005)
12. Bosse, T., Kleiser, L., Meiburg, E.: Phys. Fluids **18**, 027102 (2006)
13. Loisel, V., Abbas, M., Masbernat, O., Climent, E.: Phys. Fluids **25**, 123304 (2013)
14. Picano, F., Breugem, W.P., Brandt, L.: J. Fluid Mech. **764**, 463 (2015)
15. Huck, P.D., Bateson, C., Volk, R., Cartellier, A., Bourgoin, M., Aliseda, A.: J. Fluid Mech. **846**, 1059 (2018)
16. Schneiders, L., Fröhlich, K., Meinke, M., Schröder, W.: J. Fluid Mech. **875**, 520 (2019)
17. Muramulla, P., Tyagi, A., Goswami, P.S., Kumaran, V.: J. Fluid Mech. **889**, A28 (2020)
18. Fox, R.O., Vié, A., Laurent, F.: J. Fluid Mech. **903**, A5 (2020)
19. Boniou, V., Fox, R.O., Laurent, F.: J. Computat. Phys. (2023). HAL preprint https://hal.science/hal-04037062
20. Capecelatro, J., Desjardins, O., Fox, R.O.: J. Fluid Mech. **747**, R2 (2014)
21. Panicker, N., Passalacqua, A., Fox, R.O.: Chem. Eng. Sci. **216**, 115546 (2020)
22. Fox, R.O.: J. Fluid Mech. **877**, 282 (2019)
23. Chassagne, R., Bonamy, C., Chauchat, J.: J. Fluid Mech. **964**, A27 (2023)
24. Boniou, V., Fox, R.O.: Int. J. Multiphase Flow **169**, 104591 (2023)
25. Toro, E.F.: Riemann Solvers and Numerical Methods for Fluid Dynamics: A Practical Introduction, 3rd edn. Springer, Heidelberg (2009)

26. Fox, R.O.: J. Fluid Mech. **742**, 368 (2014)
27. Fox, R.O.: Multiphase turbulence. In: Advanced Approaches in Turbulence. Theory, Modeling, Simulation, and Data Analysis for Turbulent Flows, pp. 307–371. Elsevier (2021)
28. Pope, S.B.: Turbulent Flows. Cambridge University Press, Cambridge (2000)
29. Fox, R.O.: Annu. Rev. Fluid Mech. **44**, 47 (2012)
30. Capecelatro, J., Desjardins, O., Fox, R.O.: J. Fluid Mech. **845**, 499 (2018)
31. Schneiderbauer, S.: AIChE J. **63**(8), 3544 (2017)
32. Capecelatro, J., Desjardins, O., Fox, R.O.: J. Fluid Mech. **780**, 578 (2015)
33. Baker, M.C., Fox, R.O., Kong, B., Capecelatro, J., Desjardins, O.: Phys. Rev. Fluids **5**, 074304 (2020)
34. Mehrabadi, M., Tenneti, S., Garg, R., Subramaniam, S.: J. Fluid Mech. **770**, 210 (2015)
35. Capecelatro, J., Desjardins, O., Fox, R.O.: Phys. Fluids **28**(3), 033306 (2016)
36. Capecelatro, J., Desjardins, O., Fox, R.O.: Phys. Fluids **28**(3), 033307 (2016)
37. Risso, F.: Annu. Rev. Fluid Mech. **50**, 25 (2018)